Editors' Suggestion

Search for Light Dark Matter with NA64 at CERN

Yu. M. Andreev,[1] D. Banerjee,[2] B. Banto Oberhauser,[3] J. Bernhard,[2] P. Bisio,[4,5] A. Celentano,[4] N. Charitonidis,[2] A. G. Chumakov,[1] D. Cooke,[6] P. Crivelli,[3] E. Depero,[3] A. V. Dermenev,[1] S. V. Donskov,[1] R. R. Dusaev,[1] T. Enik,[7] V. N. Frolov,[7] R. B. Galleguillos Silva,[8,9] A. Gardikiotis,[10] S. V. Gertsenberger,[7] S. Girod,[2] S. N. Gninenko,[1,*] M. Hösgen,[11] V. A. Kachanov,[1] Y. Kambar,[7] A. E. Karneyeu,[1] E. A. Kasianova,[7] G. D. Kekelidze,[7] B. Ketzer,[11] D. V. Kirpichnikov,[1] M. M. Kirsanov,[1] V. N. Kolosov,[1] V. A. Kramarenko,[1,7] L. V. Kravchuk,[1] N. V. Krasnikov,[1,7] S. V. Kuleshov,[8,9] V. E. Lyubovitskij,[1,12,9] V. Lysan,[7] A. Marini,[4] L. Marsicano,[4] V. A. Matveev,[7] R. Mena Fredes,[9,12] R. G. Mena Yanssen,[9,12] L. Molina Bueno,[13] M. Mongillo,[3] D. V. Peshekhonov,[7] V. A. Polyakov,[1] B. Radics,[14] K. M. Salamatin,[7] V. D. Samoylenko,[1] H. Sieber,[3] D. A. Shchukin,[1] O. Soto,[15,9] V. O. Tikhomirov,[1] I. V. Tlisova,[1] A. N. Toropin,[1] M. Tuzi,[13] B. I. Vasilishin,[1] P. V. Volkov,[7] V. Yu. Volkov,[1] I. V. Voronchikhin,[1] J. Zamora-Saá,[8,9] and A. S. Zhevlakov[7]

(NA64 Collaboration)

[1]*Authors affiliated with an institute covered by a cooperation agreement with CERN*
[2]*CERN, European Organization for Nuclear Research, CH-1211 Geneva, Switzerland*
[3]*ETH Zürich, Institute for Particle Physics and Astrophysics, CH-8093 Zürich, Switzerland*
[4]*INFN, Sezione di Genova, 16147 Genova, Italia*
[5]*Università degli Studi di Genova, 16126 Genova, Italia*
[6]*UCL Departement of Physics and Astronomy, University College London, Gower St. London WC1E 6BT, United Kingdom*
[7]*Authors affiliated with an international laboratory covered by a cooperation agreement with CERN*
[8]*Center for Theoretical and Experimental Particle Physics, Facultad de Ciencias Exactas, Universidad Andres Bello, Fernandez Concha 700, Santiago, Chile*
[9]*Millennium Institute for Subatomic Physics at High-Energy Frontier (SAPHIR), Fernandez Concha 700, Santiago, Chile*
[10]*Physics Department, University of Patras, 265 04 Patras, Greece*
[11]*Universität Bonn, Helmholtz-Institut für Strahlen-und Kernphysik, 53115 Bonn, Germany*
[12]*Universidad Técnica Federico Santa María and CCTVal, 2390123 Valparaíso, Chile*
[13]*Instituto de Fisica Corpuscular (CSIC/UV), Carrer del Catedratic Jose Beltran Martinez, 2, 46980 Paterna, Valencia, Spain*
[14]*York University, Toronto, Canada*
[15]*Departamento de Fisica, Facultad de Ciencias, Universidad de La Serena, Avenida Cisternas 1200, La Serena, Chile*

(Received 9 July 2023; accepted 14 September 2023; published 16 October 2023)

Thermal dark matter models with particle χ masses below the electroweak scale can provide an explanation for the observed relic dark matter density. This would imply the existence of a new feeble interaction between the dark and ordinary matter. We report on a new search for the sub-GeV χ production through the interaction mediated by a new vector boson, called the dark photon A', in collisions of 100 GeV electrons with the active target of the NA64 experiment at the CERN SPS. With 9.37×10^{11} electrons on target collected during 2016–2022 runs NA64 probes for the first time the well-motivated region of parameter space of benchmark thermal scalar and fermionic dark matter models. No evidence for dark matter production has been found. This allows us to set the most sensitive limits on the A' couplings to photons for masses $m_{A'} \lesssim 0.35$ GeV, and to exclude scalar and Majorana dark matter with the $\chi - A'$ coupling $\alpha_D \leq 0.1$ for masses $0.001 \lesssim m_\chi \lesssim 0.1$ GeV and $3m_\chi \leq m_{A'}$.

DOI: 10.1103/PhysRevLett.131.161801

Thermal light dark matter (LDM) with DM particle (χ) masses below the electroweak scale, $m_\chi \ll 100$ GeV, is one of the most popular candidates to explain the origin of DM. In this model, dark and ordinary matter were initially in thermal equilibrium and annihilate to each other at equal rates. However, as the Universe was expanding and cooling down, the annihilation rates fell out of equilibrium and the

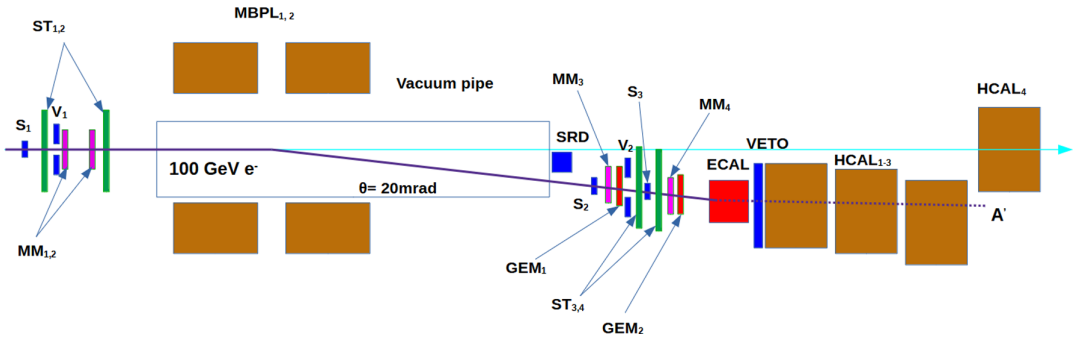

FIG. 1. Schematic illustration of the setup to search for $A' \to$ invisible decays of the bremsstrahlung A's produced in the reaction $eZ \to eZA'$ of 100 GeV e^- incident on the active ECAL target in 2021–2022 runs.

DM number density froze out at the value when equilibrium was lost. In this scenario, the existence of a new interaction between the χ and the standard model (SM) is required to accommodate the relic DM density [1,2]. In one of the most interesting cases, this interaction could be transmitted by a new vector boson, called the dark photon (A'). The A' could have a mass in the sub-GeV mass range, and coupling to photon via the kinetic mixing term $(\epsilon/2)F'_{\mu\nu}F^{\mu\nu}$. Here, $F_{\mu\nu}$ and $F'_{\mu\nu}$ are the stress tensors of the photon and dark photon fields and ϵ is the mixing strength [3–6]. The massive A'_μ field, associated with the spontaneously broken $U_D(1)$ gauge group, has the dark coupling strength e_D [of the $U_D(1)$ gauge interactions] to χ, which is given by $\mathcal{L}_{\rm int} = -e_D A'_\mu J^\mu_D$, where J_D is the dark matter current. The mixing term results in the interaction $\mathcal{L}_{\rm int} = \epsilon e A'_\mu J^\mu_{em}$ of the A' with the electromagnetic (em) current $J^\mu_{\rm em}$ with a strength ϵe, where e is the em coupling and $\epsilon \ll 1$ [7–9].

If the A' is the lightest state in the dark sector, then it would decay mostly to a visible state, i.e., to SM leptons or hadrons [10–18]. However, if the decay $A' \to \chi\chi$ is kinematically allowed, the A' would dominantly decay invisibly into χ's provided $m_\chi < m_{A'}/2$ and $e_D > \epsilon e$. Various LDM models motivate the existence of sub-GeV χ's which could be either scalar, Majorana, or pseudo-Dirac particles coupled to the A' [19–25]. Models introducing the invisible A', i.e., that invisible decay mode is dominant, $\Gamma(A' \to \bar{\chi}\chi)/\Gamma_{\rm tot} \simeq 1$, are subject to various experimental probes leaving, however, a large parameter area still to be explored.

Imposing the thermal freeze-out condition of DM annihilation into visible sector through $\gamma - A'$ mixing allows one to predict values of the parameter

$$y = \alpha_D \epsilon^2 \left(\frac{m_\chi}{m_{A'}}\right)^4, \quad (1)$$

which defines the annihilation cross section and hence the relic DM density, and also relates the dark coupling $\alpha_D = e_D^2/4\pi$ and mixing ϵ by

$$\alpha_D \simeq 0.02 f \left(\frac{10^{-3}}{\epsilon}\right)^2 \left(\frac{m_{A'}}{100\ \text{MeV}}\right)^4 \left(\frac{10\ \text{MeV}}{m_\chi}\right)^2, \quad (2)$$

where the parameter f depends on $m_{A'}$ and m_χ [1]. For $(m_{A'}/m_\chi) = 3$, $f \lesssim 10$ for the scalar [21], and $f \lesssim 1$ for the fermion case [22]. The accessibility of the predicted y and α_D values in direct searches and at accelerator experiments motivates a worldwide effort towards study of dark forces and other portals between the visible and dark sectors; see, e.g., Refs. [21,26–52].

In this Letter, we report new results on the search for the invisible A' mediator and light-dark matter in the fixed-target experiment NA64 at the CERN SPS [53,54], obtained from the combined statistics of 2016-2022 runs. The search method, proposed in Refs. [55,56], is based on the detection of missing energy, arising from prompt decays $A' \to \chi\chi$ of the hard bremsstrahlung A' produced in the process $e^-Z \to e^-ZA'$ of high-energy electrons scattering in the active beam dump target. Another A' production mechanism considered in this work allowing a large increase in the sensitivity, in particular, for the high-mass region, $m_{A'} \gtrsim m_\mu$, is through the resonant annihilation of secondary positrons from the em shower developed in the target with its atomic electrons, $e^+e^- \to A' \to \chi\chi$ [57,58]. The advantage of the NA64 approach compared to a classical beam dump experiment [21,22,40,43,59,60] is that its sensitivity is proportional to ϵ^2, while in the latter case, it is proportional to $\epsilon^4\alpha_D$ [55].

The NA64 detector upgraded for a more sensitive LDM search in 2021–2022 runs is schematically shown in Fig. 1. It employs the optimized H4 100 GeV electron beam at the CERN SPS, which has a maximal intensity $\simeq 10^7$ electrons per SPS spill of 4.8 s [61]. The beam is defined by the scintillator (Sc) counters S_{1-3} and a veto counter V_1. A magnetic spectrometer is used to reconstruct the momentum of the incoming e^-'s with the precision $\delta p/p \simeq 1\%$ [62]. The spectrometer consists of two consecutive dipole magnets $\text{MBPL}_{1,2}$ with the total magnetic field of $\simeq 7\ \text{T} \cdot \text{m}$ and a low-material-budget tracker composed of a set of two upstream Micromegas ($\text{MM}_{1,2}$) and two straw-tube

chambers ($ST_{1,2}$) and two downstream MM_{3-4}, $ST_{3,4}$, and gas electron multiplier ($GEM_{1,2}$) stations. The synchrotron radiation (SR) emitted in the MBPL magnetic field and detected with an SR detector (SRD) was used for electron identification. The SRD is an array of a PbSc sandwich calorimeter of a fine segmentation [55,63]. With this technique the initial admixture of the hadron contamination in the beam $\pi/e^- \lesssim 10^{-2}$ was further suppressed to $\simeq 2 \times 10^{-5}$ [64]. Downstream the setup was equipped with an active dump target, an em calorimeter (ECAL), for measurement of the recoil electron energy $E_{\rm ECAL}$ and the transverse and longitudinal shape of the corresponding em shower. The ECAL was a matrix of 5×6 Shashlik-type modules assembled from Pb and Sc plates of $\simeq$40 radiation lengths (X_0), with the first $4X_0$ serving as a preshower detector. Finally, the ECAL is followed by a high-efficiency veto counter VETO, and a massive, hermetic hadronic calorimeter (HCAL) of three modules $HCAL_{1-3}$, $\sim$30 nuclear interaction lengths in total to veto muons or hadronic secondaries produced in the e^- nuclei interactions in the target. A zero-degree $HCAL_4$ is used to reject beam electrons accompanied by neural secondaries.

Our data were collected during two periods with the trigger requiring the ECAL energy $E_{\rm ECAL} \lesssim 90$ GeV. The first period of 2016-2018 runs (hereafter called, respectively, runs I–III) had 2.83×10^{11} electrons on target (EOT) [47,48]. The second, the 2021 (run IV) [65] and 2022 (run V) runs, had 6.54×10^{11} EOT collected with the beam intensity in the range $\simeq(5$–$7) \times 10^6$ e^- per spill. Data with a total of 9.37×10^{11} EOT from these five runs were processed with selection criteria and combined as described below.

A GEANT4 [66,67] based Monte Carlo (MC) simulation package DMG4 [68] is used to study the performance of the detector, selection of cuts, signal acceptance, and background level. To maximize the signal acceptance and to minimize background, the following selection criteria were used: (i) The incoming track should have the momentum 100 ± 10 GeV. (ii) The deflected track angle should be within 3 mrad to reject events from the upstream e^- interactions. (iii) The detected SR energy should be within the range $\simeq$1–100 MeV emitted by e^-s and in time with the trigger. (iv) The longitudinal and lateral shape of the ECAL cluster should be consistent with the one expected for the signal event [69]. (v) There should be no multiple hits in the $ST_{3,4}$ chambers and no activity in VETO. This was an effective cut against the electroproduction of charged secondaries in the upstream beam material. The measured distribution of $\simeq 9.6 \times 10^5$ events in the ($E_{\rm ECAL}$;$E_{\rm HCAL}$) plane that passed these criteria from combined runs IV and V is shown in Fig. 2. An event was considered as a candidate for the signal if it had the missing energy $E_{\rm miss} \gtrsim 50$ GeV, here $E_{\rm miss} = E - E_{\rm ECAL} - E_{\rm HCAL}$, and E is the energy of the incoming track. The optimal boundary of the signal box ($E_{\rm ECAL} < E^{sb}_{\rm ECAL}$; $E_{\rm HCAL} < E^{sb}_{\rm HCAL}$) for the ECAL, $E^{sb}_{\rm ECAL} = 47$–50 GeV, was defined based on the energy spectrum calculations for A's emitted by $e^{\pm}$ from the e-m shower generated by the primary e^-s in the target [69,70] and the expected background level for each particular run, as described below. The optimal cut $E^{sb}_{\rm HCAL} = 1$ GeV for all runs was determined by the HCAL noise. Events originated from the rare QED dimuon production in the target were used as a reference reaction allowing us to verify the MC simulation, and cross-check systematic uncertainties and background estimate [47,48]. The A' acceptance was evaluated from simulations and e^- data sample taking into account the selection efficiency for the longitudinal and transverse em shower shape in the target arising from signal events [69]. The energy corrections were obtained from ECAL spectra of recoil e^- from dimuon events. The A' production cross section for the bremsstrahlung reaction were calculated in Ref. [70] with uncertainty $\simeq$10% [47,48], while for the resonant process was obtained as described in Ref. [58].

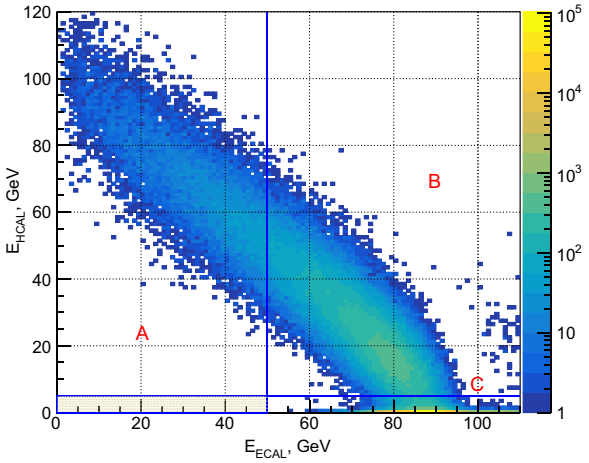

FIG. 2. The measured distribution of events in the ($E_{\rm ECAL}$;$E_{\rm HCAL}$) plane after applying all selection criteria. The shaded area is the signal box, with the size along the $E_{\rm HCAL}$ axis increased for illustration purposes. The side bands A and C are the ones used for the background estimate inside the signal region.

Several processes shown in Table I contribute to background: (i) Dimuon losses due to their inefficient detection or decays in the target. It was estimated from the measurements of the single muon efficiency. (ii) Decays of mistagged μ, π, K. It was evaluated from the simulations and measurements of the beam composition [64]. (iii) Escaping neutrals from the electroproduction in the beam line due to insufficient HCAL coverage. Compared to the first period of data taking, this background was significantly reduced by increasing the HCAL acceptance by moving it $\simeq$3 m upstream, and by decreasing the amount of dead material

TABLE I. Expected background for 2021–2022 runs.

Background source	Background, n_b
(i) dimuon losses or decays in the target	0.04 ± 0.01
(ii) $\mu, \pi, K \to e + \ldots$. decays in the beam line	0.3 ± 0.05
(iii) lost γ, n, K^0 from upstream interactions	0.16 ± 0.12
(iv) Punchthrough leading n, K_L^0	< 0.01
Total n_b (conservatively)	0.51 ± 0.13

in the beam line. (iv) Punchthrough of leading neutral hadrons (n, K_L^0) from the e^- interactions in the target. It was evaluated from the direct measurements of punchthrough events [71]. Background from the region A in Fig. 2 was found to be negligible. After applying the selection cuts, we expected mostly background events of type (iii) to remain in the data. Their number was evaluated from the data itself by the extrapolation of events from the sideband C ($E_{\rm ECAL} > E^{sb}_{\rm ECAL}; E_{\rm HCAL} < 1$ GeV) into the signal region and assessing the systematic errors by varying the fit functions. The shape of the extrapolation functions defined by events of type (iii), with a small admixture of those falling from B to C due to the HCAL energy resolution, was taken from the analysis of the data and cross-checked with simulations. Finally, the estimated background inside the signal region was 0.51 ± 0.13 events. Compared to the 2016–2018 runs [48], background was further rejected by a factor $\simeq 6$. After determining all the selection criteria and background levels, no event is found in the signal region.

To obtain upper limits on the mixing strength, runs I–V were analyzed simultaneously using the technique of multibin limit setting based on the ROOSTATS package [72]. First, the background levels, efficiencies, their corrections and uncertainties were used to optimize the ECAL energy cut for the signal box, by comparing sensitivities, defined as an average expected bound calculated using the profile likelihood ratio method for each run. For the data samples from the 2016–2021 runs we used the previously optimized value of the ECAL energy cut of 50 GeV [47,48,65]. For the 2022 run, the optimal cut was selected in the range 47–50 GeV, slightly depending on the run conditions and detector performance during the data taking. The VETO (0.94) and HCAL (0.95) efficiencies were defined as a fraction of events below the zero-energy thresholds, with the loss mostly due to pileup in high-intensity runs. The overall signal reconstruction efficiency was in the range 0.4–0.5.

The combined 90% confidence level (C.L.) upper limits for mixing strength ϵ is obtained by applying the modified frequentist approach for confidence levels, considering the profile likelihood ratio as a test statistic in the asymptotic approximation [73–75]. The number of events

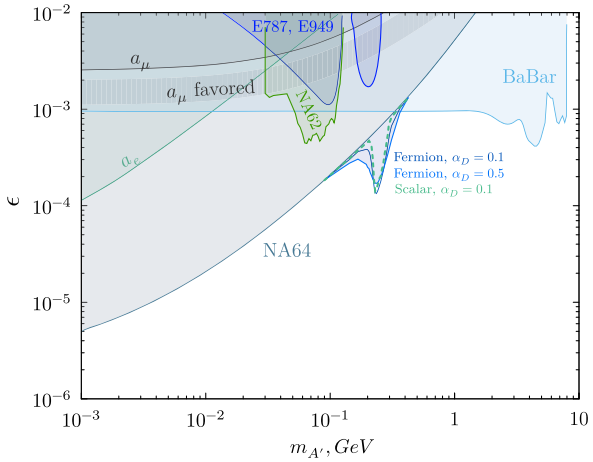

FIG. 3. The NA64 90% C.L. exclusion region in the $(m_{A'}, \epsilon)$ plane. Constraints from the E787 and E949 [41,42], *BABAR* [49], and NA62 [50] experiments, from the consideration of the anomalous magnetic moment of electron α_e [76–79], as well as the favored area explaining the α_μ anomaly with the A' contribution [10] are also shown. For more limits from indirect searches and planned measurements see, e.g., Refs. [28–30,51,52].

in the signal box is the sum of expected events from all five runs:

$$N_{A'} = \sum_{i=1}^{5} N^i_{A'} = \sum_{i=1}^{5} n^i_{\rm EOT} \epsilon^i_{A'} n^i_{A'}(\epsilon, m_{A'}, \Delta E_e), \quad (3)$$

where $n^i_{\rm EOT}$ and $\epsilon^i_{A'}$ are is the number of EOT and the signal efficiency in run i, respectively, and $n^i_{A'}(\epsilon, m_{A'}, \Delta E_e)$ is the number of signal events per EOT produced in the energy interval ΔE_e. Signal events for each ith entry in Eq. (3) are simulated and reconstructed with the same selection criteria and efficiency corrections as for the data sample from run i. The combined 90% C.L. exclusion limits on ϵ as a function of the A' mass, calculated by taking into account the estimated backgrounds and systematic errors $\sim 15\%$ for the $\epsilon^i_{A'}$—dominated by the $\sim 10\%$ uncertainty in the A' yield [47]—can be seen in Fig. 3.

Using obtained limits, Eqs. (1) and (2), one can get constraints on the LDM models, which are shown in the $(y; m_\chi)$ and $(\alpha_D; m_\chi)$ planes in Fig. 4 for $m_\chi \lesssim 1$ GeV. The favored y parameter curves for scalar, pseudo-Dirac (with a small splitting) and Majorana scenario of LDM calculated from the observed relic DM density [38] are also shown. One can see that our results are already starting to probe the $(y; m_\chi)$ parameter space predicted for the benchmark values $\alpha_D = 0.1$ and $m_{A'} = 3m_\chi$ [29,30] providing the best limits in comparison with bounds from other experiments, while leaving $\alpha_D = 0.5$ still compatible with the constraints from consideration of the running α_D [70,80]. The limits on α_D for the pseudo-Dirac (Majorana) case shown in Fig. 4 were calculated by using $f = 0.25$ ($f = 3$) in Eq. (2), see Ref. [48].

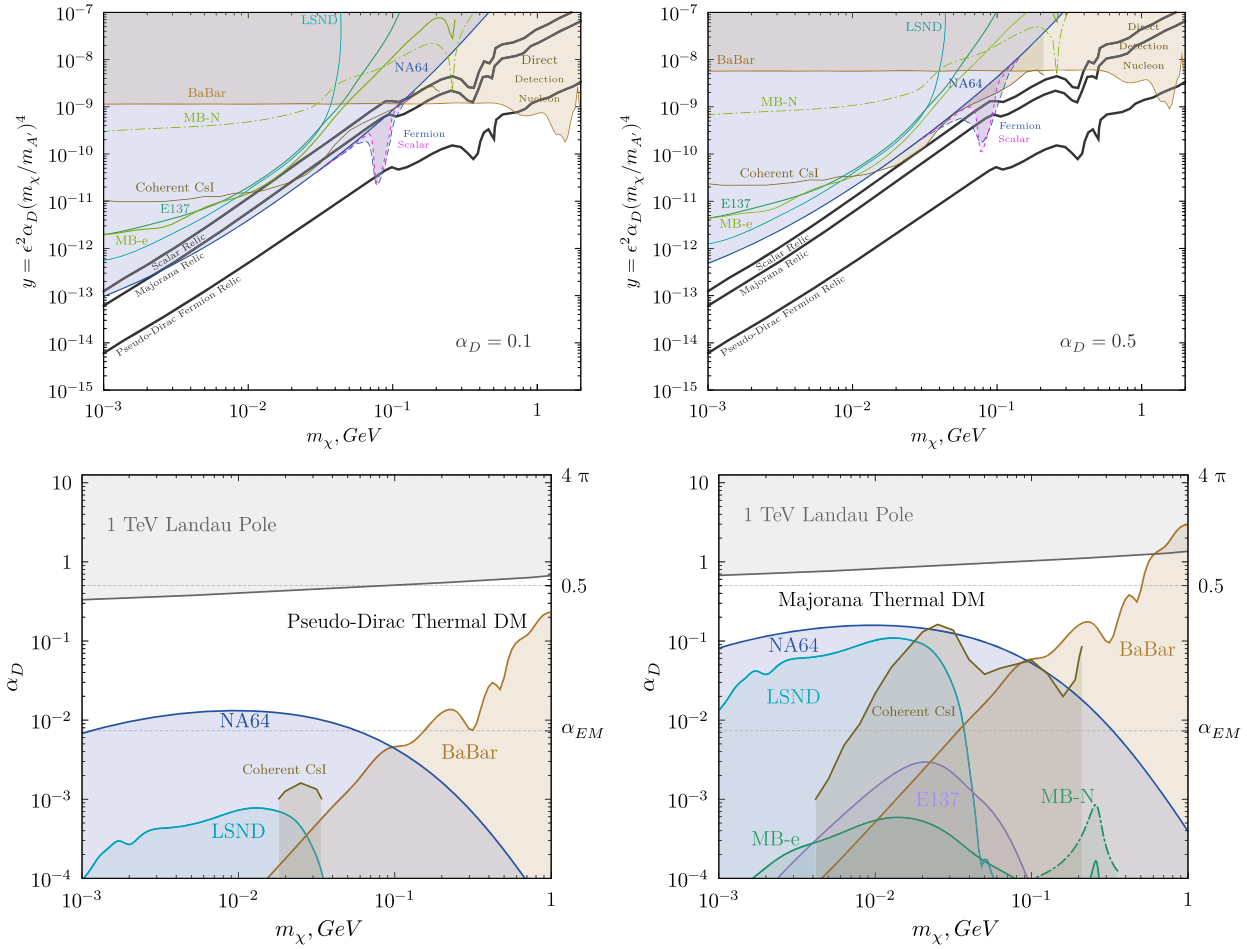

FIG. 4. The top row shows the NA64 limits in the (y;m_χ) plane obtained for $\alpha_D = 0.1$ (left panel) and $\alpha_D = 0.5$ (right panel) assuming $m_{A'} = 3m_\chi$, from the full 2016–2022 dataset. The bottom row shows the NA64 constraints in the (α_D;m_χ) plane on the pseudo-Dirac (left panel) and Majorana (right panel) DM. The limits are shown in comparison with bounds obtained in Refs. [22–24,28,29] from the results of the LSND [21,43], E137 [44], MiniBooNE [46], BABAR [49], COHERENT [81], and direct detection [82] experiments. The favored parameters to account for the observed relic DM density for the scalar, pseudo-Dirac, and Majorana type of light DM are shown as the lowest solid line in top plots; see, e.g., [38].

In summary, using the pioneering approach with the combined statistics of the 2016–2022 runs, NA64 has started probing the well-motivated region of the LDM parameter space. The world-leading bounds on ϵ, y, α_D in the mass range $0.001 \lesssim m_{A'} \lesssim 0.35$ GeV are placed [10], allowing to exclude scalar and Majorana dark matter with the $\chi - A'$ coupling $\alpha_D \leq 0.1$ for masses $0.001 \lesssim m_\chi \lesssim 0.1$ GeV and $3m_\chi \leq m_{A'}$.

We gratefully acknowledge the support of the CERN management and staff, as well as contributions from HISKP, University of Bonn (Germany), ETH Zurich, and SNSF Grants No. 169133, No. 186181, No. 186158, No. 197346 (Switzerland), ANID—Millennium Science Initiative Program—ICN2019 044 (Chile), RyC-030551-I and PID2021-123955NA-100 funded by MCIN/AEI/FEDER, UE (Spain). This result is part of a project that has received funding from the European Research Council (ERC) under the European Union's Horizon 2020 research and innovation programme, Grant Agreement No. 947715 (POKER).

*Corresponding author: sergei.gninenko@cern.ch

[1] E. W. Kolb and M. S. Turner, Front. Phys. **69**, 1 (1990).
[2] V. A. Rubakov and D. S. Gorbunov, *Introduction to the Theory of the Early Universe: Hot Big Bang Theory* (World Scientific, Singapore, 2017), p. 596.
[3] P. Fayet, Phys. Lett. **95B**, 285 (1980).
[4] M. Pospelov, A. Ritz, and M. B. Voloshin, Phys. Lett. B **662**, 53 (2008).
[5] N. Arkani-Hamed, D. P. Finkbeiner, T. R. Slatyer, and N. Weiner, Phys. Rev. D **79**, 015014 (2009).
[6] J. Jaeckel and A. Ringwald, Annu. Rev. Nucl. Part. Sci. **60**, 405 (2010).

[7] L. B. Okun, Zh. Eksp. Teor. Fiz. **83**, 892 (1982) [Sov. Phys. JETP **56**, 502 (1982)].
[8] P. Galison and A. Manohar, Phys. Lett. **136B**, 279 (1984).
[9] B. Holdom, Phys. Lett. **166B**, 196 (1986).
[10] R. L. Workman *et al.* (Particle Data Group), Prog. Theor. Exp. Phys. **2022**, 083C01 (2022).
[11] S. Abrahamyan *et al.* (APEX Collaboration), Phys. Rev. Lett. **107**, 191804 (2011).
[12] H. Merkel *et al.*, Phys. Rev. Lett. **112**, 221802 (2014).
[13] J. P. Lees *et al.* (*BABAR* Collaboration), Phys. Rev. Lett. **113**, 201801 (2014).
[14] A. Adare *et al.* (PHENIX Collaboration), Phys. Rev. C **91**, 031901 (2015).
[15] J. R. Batley *et al.* (NA48/2 Collaboration), Phys. Lett. B **746**, 178 (2015).
[16] A. Anastasi *et al.* (KLOE-2 Collaboration), Phys. Lett. B **757**, 356 (2016).
[17] D. Banerjee *et al.* (NA64 Collaboration), Phys. Rev. Lett. **120**, 231802 (2018).
[18] D. Banerjee *et al.* (NA64 Collaboration), Phys. Rev. D **101**, 071101 (2020).
[19] P. Fayet, Phys. Rev. D **75**, 115017 (2007).
[20] M. Pospelov, Phys. Rev. D **80**, 095002 (2009).
[21] P. deNiverville, M. Pospelov, and A. Ritz, Phys. Rev. D **84**, 075020 (2011).
[22] E. Izaguirre, G. Krnjaic, P. Schuster, and N. Toro, Phys. Rev. D **91**, 094026 (2015).
[23] E. Izaguirre, G. Krnjaic, P. Schuster, and N. Toro, Phys. Rev. Lett. **115**, 251301 (2015).
[24] E. Izaguirre, Y. Kahn, G. Krnjaic, and M. Moschella, Phys. Rev. D **96**, 055007 (2017).
[25] P. J. Fitzpatrick, H. Liu, T. R. Slatyer, and Y.-D. Tsai, Phys. Rev. D **106**, 083517 (2022).
[26] A. Boveia *et al.*, arXiv:2210.01770.
[27] R. Essig *et al.*, arXiv:1311.0029.
[28] J. Alexander *et al.*, arXiv:1608.08632.
[29] M. Battaglieri *et al.*, arXiv:1707.04591.
[30] J. Beacham *et al.*, J. Phys. G **47**, 010501 (2020).
[31] R. Alemany *et al.*, arXiv:1902.00260.
[32] P. Agraval *et al.*, Eur. Phys. J. C **81**, 1015 (2021).
[33] R. Essig, Y. Kahn, S. Knapen, A. Ringwald, and N. Toro, arXiv:2203.10089.
[34] B. Batell, N. Blinov, Ch. Hearty, and R. McGehee, arXiv:2207.06905.
[35] S. Gori *et al.*, arXiv:2209.04671.
[36] G. Lanfranchi, M. Pospelov, and Ph. Schuster, Annu. Rev. Nucl. Part. Sci. **71**, 279 (2021).
[37] M. Fabbrichesi, E. Gabrielli, and G. Lanfranchi, arXiv:2005.01515.
[38] A. Berlin, N. Blinov, G. Krnjaic, P. Schuster, and N. Toro, Phys. Rev. D **99**, 075001 (2019).
[39] H. S. Lee, Phys. Rev. D **90**, 091702(R) (2014).
[40] M. D. Diamond and P. Schuster, Phys. Rev. Lett. **111**, 221803 (2013).
[41] H. Davoudiasl, H. S. Lee, and W. J. Marciano, Phys. Rev. D **89**, 095006 (2014).
[42] R. Essig, J. Mardon, M. Papucci, T. Volansky, and Y. M. Zhong, J. High Energy Phys. 11 (2013) 167.
[43] B. Batell, M. Pospelov, and A. Ritz, Phys. Rev. D **80**, 095024 (2009).
[44] B. Batell, R. Essig, and Z. Surujon, Phys. Rev. Lett. **113**, 171802 (2014).
[45] D. Banerjee *et al.* (NA64 Collaboration), Phys. Rev. Lett. **118**, 011802 (2017).
[46] A. A. Aguilar-Arevalo *et al.* (MiniBooNE Collaboration), Phys. Rev. D **98**, 112004 (2018).
[47] D. Banerjee *et al.* (NA64 Collaboration), Phys. Rev. D **97**, 072002 (2018).
[48] D. Banerjee *et al.* (NA64 Collaboration), Phys. Rev. Lett. **123**, 121801 (2019).
[49] J. P. Lees *et al.* (*BABAR* Collaboration), Phys. Rev. Lett. **119**, 131804 (2017).
[50] E. Cortina Gil *et al.* (NA62 Collaboration), J. High Energy Phys. 05 (2019) 182.
[51] D. McKeen, D. E. Morrissey, M. Pospelov, H. Ramani, and A. Ray, Phys. Rev. Lett. **131**, 011005 (2023).
[52] B. Dutta, W.-C. Huang, and J. L. Newstead, Phys. Rev. Lett. **131**, 111801 (2023).
[53] S. N. Gninenko, N. V. Krasnikov, and V. A. Matveev, Usp. Fiz. Nauk **191**, 1361 (2021).
[54] P. Crivelli, arXiv:2301.09905.
[55] S. N. Gninenko, Phys. Rev. D **89**, 075008 (2014).
[56] S. Andreas *et al.*, arXiv:1312.3309.
[57] L. Marsicano, M. Battaglieri, M. Bondi, C. D. R. Carvajal, A. Celentano, M. De Napoli, R. De Vita, E. Nardi, M. Raggi, and P. Valente, Phys. Rev. Lett. **121**, 041802 (2018).
[58] Yu. M. Andreev *et al.* (NA64 Collaboration), Phys. Rev. D **104**, L091701 (2021).
[59] S. N. Gninenko, Phys. Rev. D **85**, 055027 (2012).
[60] S. N. Gninenko, Phys. Lett. B **713**, 244 (2012).
[61] See, for example, http://sba.web.cern.ch/sba/.
[62] D. Banerjee, P. Crivelli, and A. Rubbia, Adv. High Energy Phys. **2015**, 105730 (2015).
[63] E. Depero *et al.*, Nucl. Instrum. Methods Phys. Res., Sect. A **866**, 196 (2017).
[64] Yu. M. Andreev *et al.* (NA64 Collaboration), arXiv:2305.19411.
[65] Yu. M. Andreev *et al.* (NA64 Collaboration), Phys. Rev. Lett. **129**, 161801 (2022).
[66] S. Agostinelli *et al.* (GEANT4 Collaboration), Nucl. Instrum. Methods Phys. Res., Sect. A **506**, 250 (2003).
[67] J. Allison *et al.*, IEEE Trans. Nucl. Sci. **53**, 270 (2006).
[68] M. Bondi, A. Celentano, R. R. Dusaev, D. V. Kirpichnikov, M. M. Kirsanov, N. V. Krasnikov, L. Marsicano, and D. Shchukin, Comput. Phys. Commun. **269**, 108129 (2021).
[69] S. N. Gninenko, N. V. Krasnikov, M. M. Kirsanov, and D. V. Kirpichnikov, Phys. Rev. D **94**, 095025 (2016).
[70] S. N. Gninenko, D. V. Kirpichnikov, M. M. Kirsanov, and N. V. Krasnikov, Phys. Lett. B **782**, 406 (2018).
[71] D. Banerjee *et al.* (NA64 Collaboration), Phys. Rev. Lett. **125**, 081801 (2020).
[72] I. Antcheva *et al.*, Comput. Phys. Commun. **180**, 2499 (2009).
[73] T. Junk, Nucl. Instrum. Methods Phys. Res., Sect. A **434**, 435 (1999).

[74] G. Cowan, K. Cranmer, E. Gross, and O. Vitells, Eur. Phys. J. C **71**, 1 (2011).
[75] A. L. Read, J. Phys. G **28**, 2693 (2002).
[76] D. Hanneke, S. Fogwell, and G. Gabrielse, Phys. Rev. Lett. **100**, 120801 (2008).
[77] R. Bouchendira, P. Clade, S. Guellati-Khelifa, F. Nez, and F. Biraben, Phys. Rev. Lett. **106**, 080801 (2011).
[78] L. Morel, Z. Yao, P. Clade, and S. Guellati-Khelifa, Nature (London) **588**, 61 (2020).
[79] T. Aoyama, M. Hayakawa, T. Kinoshita, and M. Nio, Phys. Rev. Lett. **109**, 111807 (2012).
[80] H. Davoudiasl and W. J. Marciano, Phys. Rev. D **92**, 035008 (2015).
[81] D. Akimov *et al.* (COHERENT Collaboration), Phys. Rev. Lett. **130**, 051803 (2023).
[82] R. Essig, A. Manalaysay, J. Mardon, P. Sorensen, and T. Volansky, Phys. Rev. Lett. **109**, 021301 (2012).